Ultrasonics - Sonochemistry 42 (2018) 776–786

Contents lists available at ScienceDirect

Ultrasonics - Sonochemistry

journal homepage: www.elsevier.com/locate/ultson

Ultrasound-accelerated synthesis of gold nanoparticles modified choline chloride functionalized graphene oxide as a novel sensitive bioelectrochemical sensor: Optimized meloxicam detection using CCD-RSM design and application for human plasma sample

Sonia Bahrani[a], Zahra Razmi[a], Mehrorang Ghaedi[a,*], Arash Asfaram[b], Hamedreza Javadian[c]

[a] Department of Chemistry, Yasouj University, Yasouj 75918-74831, Iran
[b] Medicinal Plants Research Center, Yasuj University of Medical Sciences, Yasuj, Iran
[c] Universitat Politècnica de Catalunya, Department of Chemical Engineering, ETSEIB, Diagonal 647, 08028 Barcelona, Spain

ARTICLE INFO

Keywords:
Bioelectrochemical sensor
Gold nanoparticles
Choline chloride
Graphene oxide
Meloxicam
Plasma

ABSTRACT

In this research, gold nanoparticles modified choline chloride functionalized graphene oxide (AuNPs-ChCl-GO) was synthesized through the assistance of ultrasound and fabricated as a novel bioelectrochemical sensor and utilized for the sensitive detection of meloxicam (MEL). The morphological and structural features of the AuNPs-ChCl-GO were characterized using different techniques including FTIR, TEM, FE-SEM, EDX, and XRD. The modified electrode showed a remarkable improvement in the anodic oxidation activity of MEL due to the enhancement in the current response compared to the bare carbon paste electrode (CPE). The biosensor composition and measurement conditions were optimized using an experimental design. The differential pulse voltammetry (DPVs) exhibited expanded linear dynamic in the range of 9.0×10^{-9} to 8.5×10^{-7} M for MEL in Britton-Robinson buffer at pH = 4.0 with a detection limit of 1.008×10^{-9} M. The practical utility of the modified electrode was demonstrated by the accurate detection of MEL in human plasma sample.

1. Introduction

The novel non-steroidal anti-inflammatory drug (NSAIDs) and COX-II inhibitor of the enolic acid oxicam derivatives, Meloxicam (MEL) (4-hydroxy-2-methyl-N-(5-methyl-2-thiazoly)-2H-1, 2-benzo-thiazine-3-carboxamide-1,1dioxide) (Fig. 1), is applied to relieve symptoms of pain and inflammation with analgesic and antipyretic properties [1–3].

Due to extremely low solubility of MEL in acidic medium, it may cause local gastrointestinal adverse events [4]. It is generally used to treat osteoarthritis and rheumatoid arthritis; however, it can be used for other painful conditions such as injuries, cancer surgery, and dental infections [5]. Up to now, spectrophotometric [6], electrophoretic [7], chromatographic [8], polarographic [9,10] methods are reported in the literatures for the analysis of MEL in pharmaceuticals. However, HPLC technique is commonly used to detect MEL in biological media [11]. Furthermore, chromatographic techniques need manipulation steps and are time-consuming. For this reason, electrochemical sensors can be noted owing to their inherent speed of response, sensitivity and simplicity of preparation. In attempt to sensitively quantify MEL concentration, the modification of graphite electrode through the introduction of other materials has considered and received the attentions of analytical researchers.

Nowadays, there has been an increasing interest in graphene-based materials that improve electronic-transfer in electrochemical sensors [12,13]. The unique properties of them can be related to their high surface area, high adsorption capacity, remarkable biocompatibility, and easy functionalization, resulting in their application in physical, chemical and biomedical fields [14]. Graphene oxide as the most popular nanomaterial contains different hydrophilic functional groups such as hydroxyl, epoxy and acidic and strongly oxygenated [15] that facilitate its dispersion in various solvents with long-term stability [16]. The investigations on GO-based electrochemical sensors have shown satisfactory and promising results for sensitive detection of drugs. In spite of the fact that pristine GO exhibits weak catalytic performance in some cases due to its poor conductivity [17], different approaches have been used by modifying the electrodes with different materials to enhance its electrochemical performance [18].

ChCl is a quaternary ammonium salt that is non-toxic, biodegradable and very cheap. In addition, whereas choline cation belongs to an important class of vitamin B family that are water-soluble vitamins and

* Corresponding author.
E-mail addresses: m_ghaedi@mail.yu.ac.ir, m_ghaedi@yahoo.com (M. Ghaedi).

https://doi.org/10.1016/j.ultsonch.2017.12.042
Received 27 November 2017; Received in revised form 20 December 2017; Accepted 21 December 2017
Available online 22 December 2017
1350-4177/

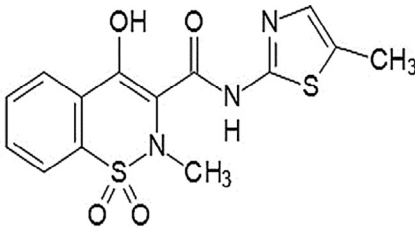

Fig. 1. Chemical structure of Meloxicam.

plays important roles in cell metabolism by assisting in various metabolic mechanisms, one of the most common components used in deep eutectic solvents (DES) is ChCl [19]. In comparison with the routine methods, the advantages of this research work are as follows: (1) the –OH group of ChCl makes it to be easily assembled onto the surface of graphene oxide sheets through covalent linkage [20] and (2) the cholinium cationic polar head group ($–N^+(CH_3)_3$) of ChCl can provide a uniform positively charged surface with a suitable density, which can facilitate the deposition of Au nanoparticles through the electrostatic interaction between $–N^+(CH_3)_3$ and $AuCl_4^-$ [21]. For these reasons, Wang et al. [22] reported a simple and sensitive AuNPs modified electrode using ChCl as a supporting material. There are some reports of using vitamins in biosystems such as electrochemical biosensor and their applications to modify ceramic and metallic particles as modification of TiO_2 nanoparticles with vitamin B_{12} for investigating the relationships between vitamin B_{12} content and its optical properties [21–26].

Among a variety of approaches, the utilization of ultrasound for materials synthesis has been extensively examined over many years, and is now positioned as one of the most powerful tools in nanostructured materials synthesis [27]. In this study, choline chloride functionalized graphene oxide modified with gold nanoparticles was synthesized by ultrasound that integrates the electrically conductivity property of graphene, hydrophilicity of choline chloride (ChCl) with active sites to immobilize the gold nanoparticles (AuNPs). The carboxylic groups of GO sheets was chemically modified by ChCl through oxygen atom via esterification reaction [28]. The covalent functionalization of graphene sheets with ChCl is shown in Scheme 1. The esterification strategy of GO with ChCl is through its acyl chloride derivative (GOCl) for the activation of the acid groups of GO using thionyl chloride ($SOCl_2$). The obtained product was named as GOCl-es-Ch. By this strategy, the selective functionalization of carboxylic acid groups of GO over other groups at their edges (according to the widely accepted Lerf–Klinowski model), and epoxy and hydroxyl groups on the basal planes is provided [29]. Experimental design is a time-saving and cost effective approach to predict, optimize and extract more information with the minimum number of experiments. Central composite design (CCD) is one of the important experimental designs that is useful for the extraction of the main and quadratic terms along with the possible interactions between variables in the process [30–33]. The electrochemical detection of MEL by AuNPs-ChCl-GO modified electrode was investigated in detail.

2. Experimental

2.1. Materials

MEL was supplied from Sigma-Aldrich, USA, with 98% purity. Britton-Robinson buffer (B-R buffer) 4.0×10^{-2} M was prepared by mixing H_3PO_4, acetic acid and boric acid with the appropriate amount of 0.2 M NaOH to obtain the desired pH. Pure graphite powder was obtained from Sigma-Aldrich, USA. Paraffin oil purchased from Merck was used as the pasting liquid for the preparation of the paste electrodes. A stock anhydrous ethanol solution of MEL (1.0×10^{-3} M) was prepared and kept in a dark place at below 4 °C. Fresh human plasma samples were provided from Fars Blood Transfusion Center (Shiraz, Fars, Iran).

2.2. Instruments and experimental conditions

The FTIR spectra of the samples were recorded by Shimadzu-FTIR-8300 spectrophotometer. X-ray diffractometer with CuKα (λ = 1.54178 Å) radiation was used. The size of the synthesized nanoparticles was confirmed by Philips CM10 transmission electron microscopy instrument. Voltammetric measurements were carried out on Autolab PGSTAT 101 Potentiostat/Galvanostat (Metrohm Autolab, Utrecht, the Netherlands) in a conventional three-electrode glass cell (volume 250 mL, Autolab, Metrohm Autolab,

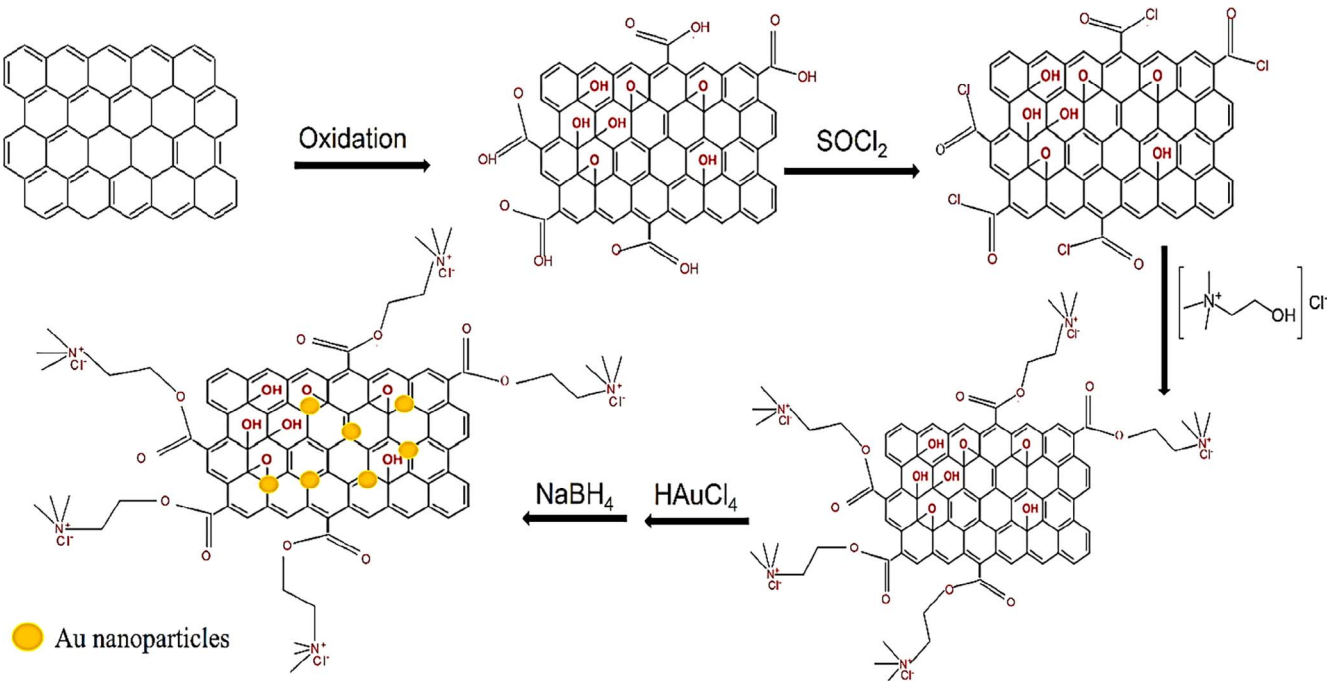

Scheme 1. Synthesis of gold nanoparticles modified choline chloride functionalized graphene oxide (AuNPs-ChCl-GO).

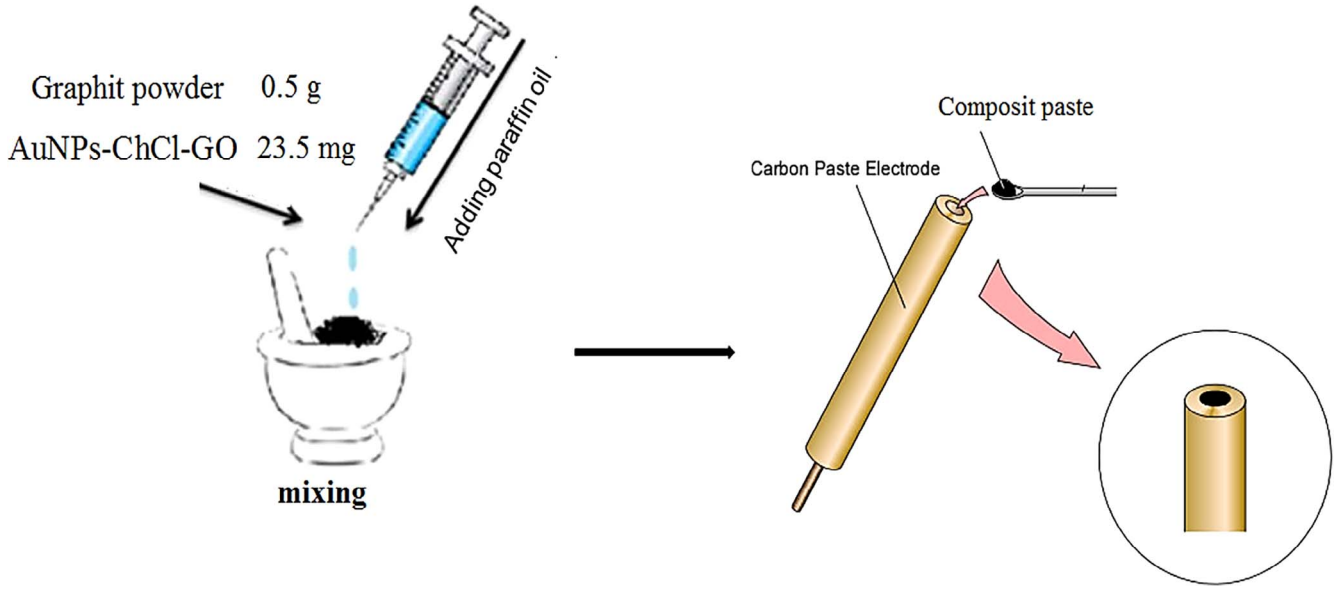

Scheme 2. Preparation of carbon paste electrode.

Table 1
Experimental parameters obtained by CCD.

Factors	Levels			Star point α = 1.7	
	Low	Central	High	−α	+α
pH of B-R buffer	3.0	5.0	7.0	1.5	8.5
Modifier quantity (mg)	10.0	15.0	20.0	6.0	24.0
Scan rate (mV/s)	20.0	30.0	40.0	12.0	48.0
Run	pH of B-R buffer	Modifier quantity (mg)	Scan rate (mV/s)	I/μA	
1	3.0	10.0	20.0	8.34	
2	3.0	10.0	40.0	6.80	
3	3.0	20.0	20.0	8.23	
4	3.0	20.0	40.0	9.80	
5	7.0	10.0	20.0	4.73	
6	7.0	10.0	40.0	3.30	
7	7.0	20.0	20.0	4.93	
8	7.0	20.0	40.0	4.80	
9	5.0	15.0	30.0	5.40	
10	1.5	15.0	30.0	7.50	
11	8.5	15.0	30.0	2.00	
12	5.0	6.0	30.0	6.12	
13	5.0	24.0	30.0	8.85	
14	5.0	15.0	12.4	6.95	
15	5.0	15.0	47.6	5.40	
16	5.0	15.0	30.0	5.20	

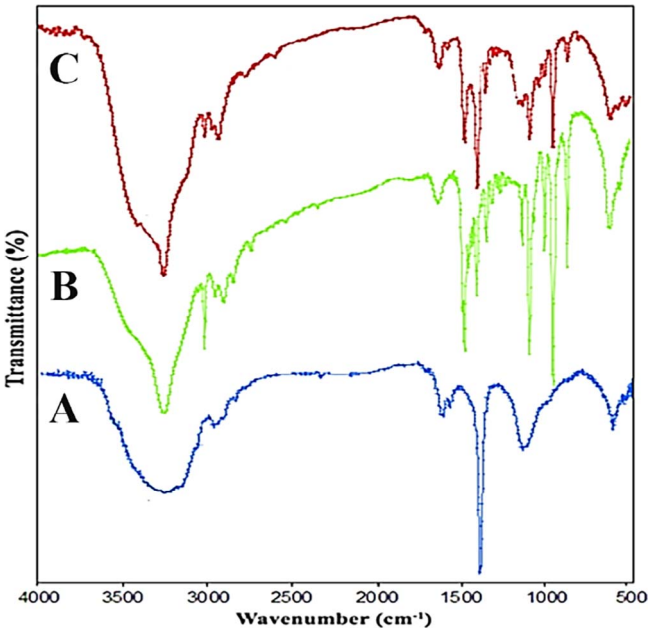

Fig. 2. FTIR spectra of (A) the GO, (B) the choline chloride, and (C) the AuNPs-ChCl-GO.

Utrecht, The Netherlands) with a triple-electrode configuration at ambient temperature of 25 ± 1 °C and controlled by Nova 1.6 software. The counter and reference electrodes were platinum (Metrohm) and Ag/AgCl (Metrohm) electrodes, respectively. Differential pulse voltammetric measurements were performed at a step potential of 5 mV, pulse height of 25 mV and pulse width of 50 ms. The shape and surface morphology of the product were investigated by field emission scanning electron microscope (FE-SEM, Hitachi S4160) under an acceleration voltage of 10 kV. The atomic composition of the product was analyzed by energy-dispersive X-ray spectrometer (EDX) using an Oxford INCA II energy solid state detector. STATISTICA software version 10.0 (Stat soft Inc., Tulsa USA) was used for experimental design analysis.

2.3. Preparation of the products

2.3.1. Preparation of the GO

The GO was prepared by a modified Hummers' method by oxidizing graphite powder [34–37] 3.0 g of the graphite powder was oxidized by 60 mL of HNO_3 and H_2SO_4 (1:3, v/v) mixture under reflux in order to form carboxyl groups on its surface. Then, the mixture was stirred for 48 h and cooled to room temperature. The solid was then centrifuged, washed with THF and dried in an oven. The pre-oxidized graphite was further oxidized by a mixture of 120 mL H_2SO_4 and 15.0 g $KMnO_4$ under reflux for 3 h. Finally, the GO was collected and dried.

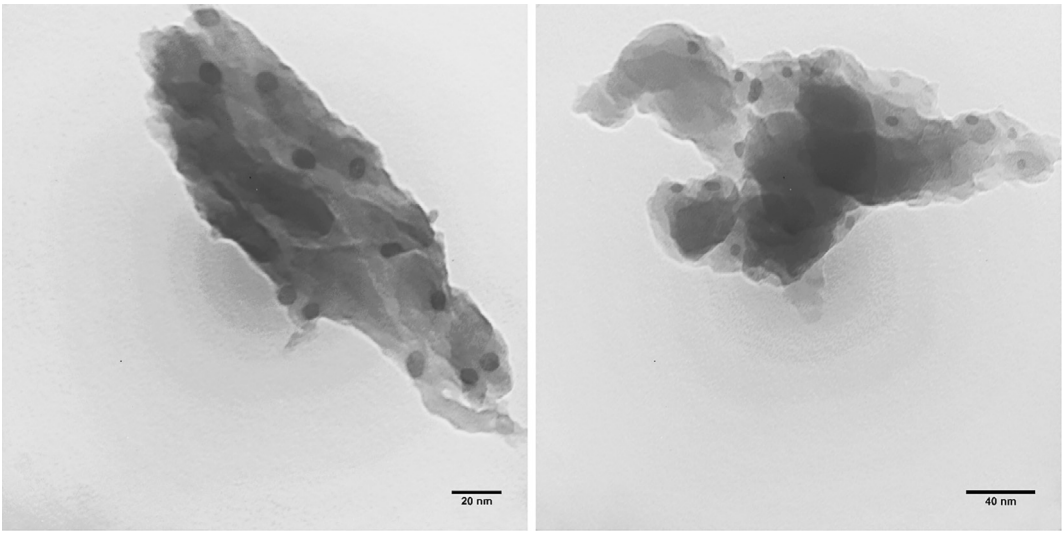

Fig. 3. TEM images of the AuNPs-ChCl-GO.

2.3.2. Acylation of the GO

1.0 g of the GO was first dispersed in 20 mL DMF under ultrasonic irradiation for 1 h and then refluxed in the presence of 60 mL $SOCl_2$ at 80 °C for 48 [38,39].

2.3.3. Preparation of the choline chloride functionalized GO

0.5 g choline chloride in 10 mL THF was added to the thionyl chloride treated GO under stirring, followed by the addition of 5 mL triethylamine. After sonication for 2 h, the reaction mixture was vigorously stirred for 36 h, leading to a dark suspension. The solid was then centrifuged, and the solvent in the clear solution was partially removed by evaporation. It was further purified by washing several times with distilled water and absolute ethanol to remove the excess trimethylamine. Finally, the product was dried in an oven at 60 °C overnight.

2.3.4. Synthesis of the AuNPs-ChCl-GO

The synthesis of the supported AuNPs was carried out in two simple steps: Firstly, the $AuCl_4^-$ anionic complex was adsorbed onto the choline chloride functionalized graphene oxide by ion-exchange reaction with the positively charged ammonium groups. The reaction was carried out by immersing 0.5 g of the functionalized GO in 50.0 mL of 0.1×10^{-3} M $HAuCl_4$ solution. The mixture was kept under stirring for 3 h at room temperature. The solid was then centrifuged and washed several times with distilled water. In the second step, the functionalized GO was immersed in 50.0 mL of 1.0×10^{-2} M $NaBH_4$ solution under sonicated for 30 min. The resulting solid was then centrifuged, washed with distilled water and finally dried at 353 K. The AuNPs-ChCl-GO synthesized in four steps mentioned above is shown in Scheme 1.

2.3.5. Preparation of the modified electrode

The unmodified carbon paste electrode (CPE) was prepared by mixing graphite 0.5 g powder with 0.3 mL paraffin oil in a glassy mortar. The carbon paste was packed into the hole of the electrode body and smoothed on a filter paper until reaching shiny appearance. To prepare nanocomposite modified electrode, the known amounts of the AuNPs-ChCl-GO were separately mixed well with 0.5 g graphite. Each AuNPs-ChCl-GO paste was mixed well with an appropriate amount of paraffin oil for 40 min until a uniform and homogeneous wetted paste was obtained (Scheme 2). These pastes were packed into the hole of the electrode body and smoothed on a filter paper until reaching shiny appearance. A new surface was obtained by pushing excess of the paste out of the syringe and polished with weighing paper.

2.3.6. Plasma sample preparation

Prior to analysis, the plasma sample was prepared by deprotonation of the plasmatic proteins by adding 0.5 mL of 2.0 M $HClO_4$ to 1.0 mL of the sample and then, it was centrifuged for 10 min at 1500 rpm. Afterwards, the supernatant was diluted five times and used for MEL analysis by standard addition method. Therefore, the prepared sample was spiked with different volumes of MEL standard solution in B-R buffer solution of pH 4.0.

2.4. Experimental design

Owing to the fact that it is difficult to simultaneously optimize the process conditions through one variable, the pH of B-R buffer (1.5–8.5), the modifier quantity (6.0–24.0 mg) and the scan rate (12–48 mV/s) were experimentally designed as indicated in Table 1. The application of CCD in RSM, was on the basis of STATISTICA software (version 10.0) to survey the effective parameters influencing the biosensor performance. The correlation between the independent variables and the response was calculated by second-order polynomial equation. Typical equation and parameters of second order polynomial model were fully presented in our previous publications [40–42]. The suitability of the response surface model was evaluated by calculating R squared and adjusted R^2. Analysis of variance (ANOVA) is a statistical method that partitions the total variation into its component parts while each term has different sources of variations and is applied for investigation of linearity, quadratic and interactions modes in a process. It was studied to evaluate the significance and adequacy of the developed model by assessing the lack of fit, regression coefficient (R^2) and the Fisher test (F-value), and *t*-test (p value $< .05$). The t-value indicates the availability of statistically difference of the means of two parameters. The larger t-value and smaller p-value approve the significance of parameters [43].

3. Results and discussions

3.1. Characterization of the products

Fig. 2 shows the FTIR spectra of GO and AuNPs-ChCl-GO to clarify

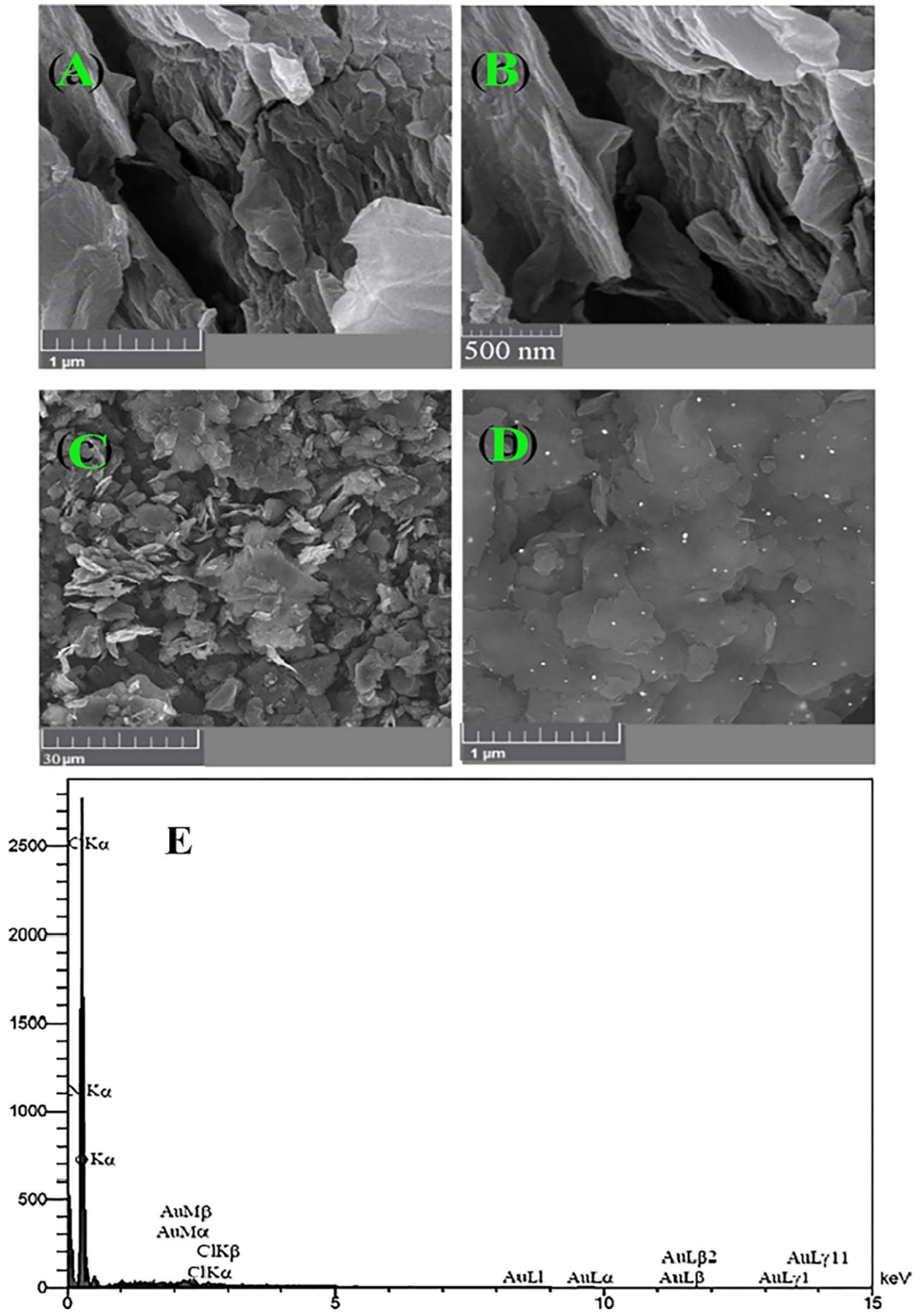

Fig. 4. SEM images of (A,B) the GO with different magnifications (C,D) the AuNPs-ChCl-GO with different magnifications and (E) EDX spectrum of the AuNPs-ChCl-GO.

the covalent linkage between GO and choline chloride. Fig. 2A indicates the characteristic bands of GO around 3446, 1725, 1620, 1405 and 1105 cm^{-1} assigned to the stretching vibration of O—H (intercalated water), C═O (carboxyl), C═C (double bond), C—OH (hydroxyl) and C—O (epoxy or alkoxy) groups, respectively [44]. The O—H and C—N vibrations of pure ChCl in Fig. 2B are positioned at 3300–3500, 1080 and 1050 cm^{-1}, respectively. The peak located at 1050 cm^{-1} is related to the C—C-O stretching vibration [44]. In addition, there are more peaks indicating the presence of a specific group of quaternary ammonium compounds in the range of 900 to 980 cm^{-1}. The asymmetric

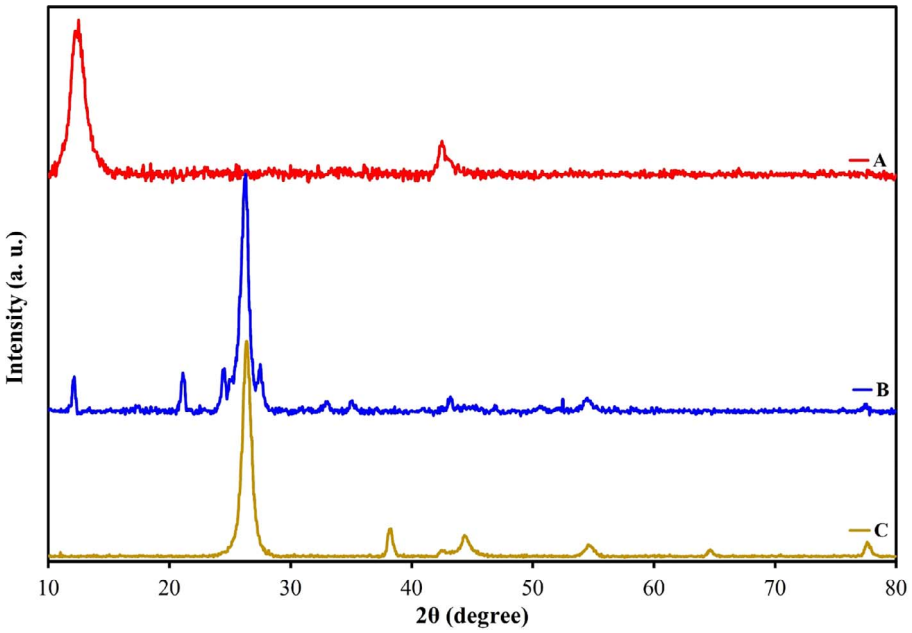

Fig. 5. XRD patterns of (A) the GO (B) the choline chloride functionalized GO (C) and the AuNPs-ChCl-GO.

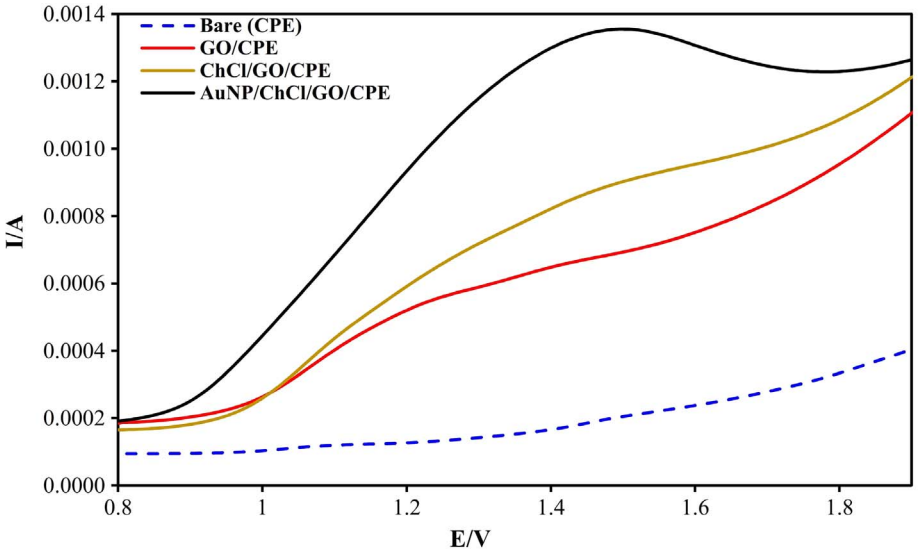

Fig. 6. Differential voltammograms of 1.0 mM MEL in the B–R buffer (pH 4.0) recorded by the CPE, GO/CPE, ChCl/GO/CPE and AuNPs/ChCl/GO/PG modified electrodes.

and symmetric stretching modes of C—N group of ChCl are located at 955 and 923 cm^{-1}, respectively [45]. The FTIR spectra of AuNPs-ChCl-GO and ChCl are shown in Fig. 2C. In comparison with ChCl, the frequency of C—C at 955 cm^{-1} is not changed that indicates the structure of Ch^{+} is not destroyed in the nanocomposite [44].

The TEM image of AuNPs-ChCl-GO in Fig. 3 shows the uniformly distributed AuNPs with average size of ~13 nm on the GO surface.

Fig. 4 demonstrates the morphology and composition of the GO and AuNPs-ChCl-GO characterized by FE-SEM and Energy-dispersive X-ray spectroscopy (EDX), respectively. The pristine GO structure is presented in Fig. 4A and B showing the typical flake like morphology in different magnifications. As shown in Fig. 4C and D, many free-standing nanosheets with the sizes of 100 nm to micrometers are observed. This change in morphology indicates the existence of Ch groups on the GO surfaces. It can be seen that the AuNPs are formed spherically and homogeneously dispersed on the surface of the ChCl-GO.

The EDX spectrum of AuNPs-ChCl-GO in Fig. 4E shows the formation of AuNPs and confirms the presence of the C, O, N, Cl, and Au elements. The nitrogen and chlorine peaks in EDX spectrum can be attributed to the presence of choline on the surface of the GO. The EDX analysis indicated that the AuNPs content in the AuNPs-ChCl-GO was ~2 wt%.

Fig. 5 shows the XRD patterns of the GO, choline chloride functionalized GO, and AuNPs-ChCl-GO. The XRD pattern of the GO in Fig. 5A shows two identical peaks at 2θ = 12.29° and 42.47° corresponding to the (0 0 2) plane of GO and (1 0 0) plane of the hexagonal structure of carbon, respectively [46]. There is a strong peak at 2θ = 12.29° showing the interlayer distance of 0.68 nm between the GO layers according to Braggs law [47]. The XRD pattern of the ChCl-GO in Fig. 5B indicates the peaks at 2θ values of 16.59°, 22.76°, 28.80°, 29.09°, 29.86°, 30.25°, 34.11°, 36.17°, 41.85°, 45.65°, 49.97°, 50.62°, 51.20°, 52.15°, 54.59°, 58.61°, 70.28° and 72.26° that are in accordance with

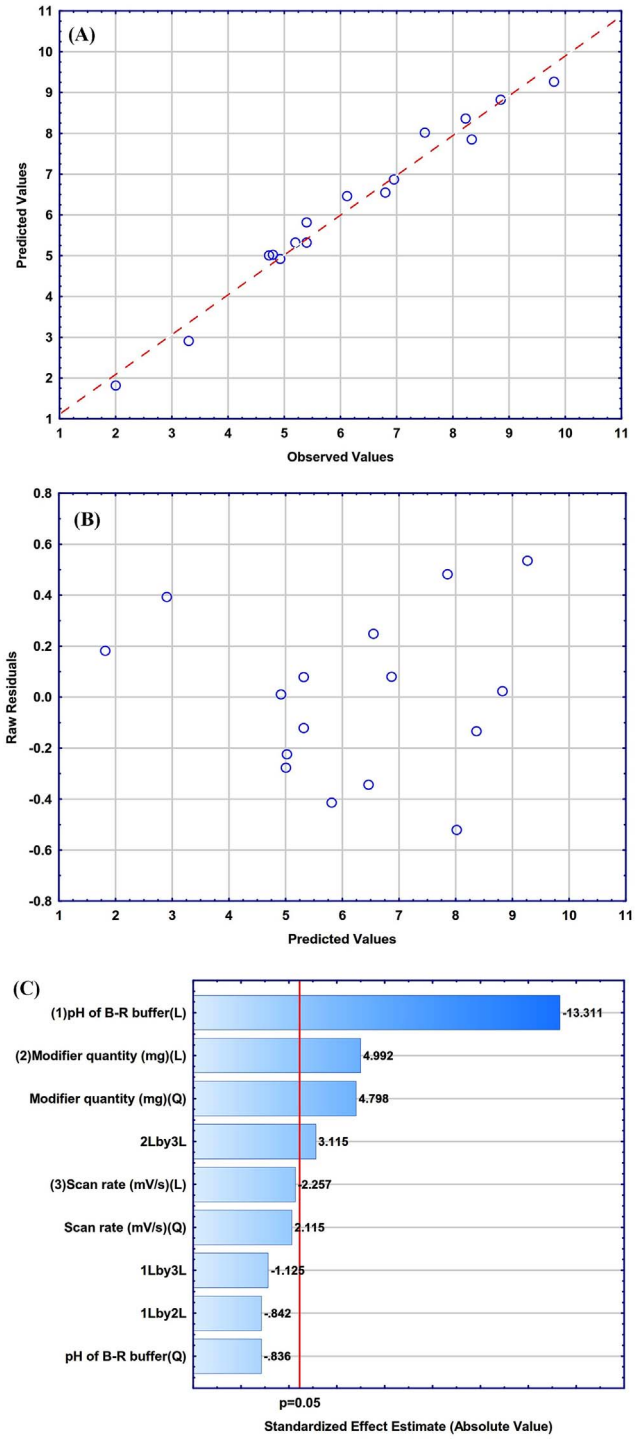

Fig. 7. (A) Linear correlation plot between actual and predicted data (B) the relationship between the residual and predicted data (C) Pareto chart for effect evaluation of the various variables on the response by the AuNPs/ChCl/GO/CPE.

the result reported in the literature [44]. However, the ChCl-GO shows the presence of peaks at 2θ values of 12.1°, 17.2°, 21.2°, 22.1°, 24.4°, 26.1°, 27.5°, 30.9°, 32.9°, 34.9°, 43.2°, 46.7°, 50.7°, 52.5°, and 54.9° indicating the interaction between the GO and choline chloride during the modification as it observed in the FTIR study as well. The obtained curve contains a weak peak at 2θ = 12.0° related to the GO. According to the Bragg equation, the distance between the GO sheets was 0.68 nm while after modification this distance reached to 0.73 nm. Increasing in distance is related to the presence of choline chloride agents on the surface of the GO sheets [48]. Fig. 5C shows the XRD pattern of the synthesized AuNPs-ChCl-GO that indicates the formation of AuNPs after reduction by $NaBH_4$ solution. The diffraction peaks at 2θ = 38.04°, 44.62°, 63.26° and 78.92° are in good accordance with the (1 1 1), (2 0 0), (2 2 0), and (3 1 1) crystallographic planes of face-centered cubic (fcc) AuNPs (JCPDS NO. 00-004-0784), respectively [49].

Table 2
Results of ANOVA for CCD.

Source	Sum of Squares	Df	Mean Square	F-Value	p-value
(1) pH of B-R solution (L)	44.32966	1	44.32966	2216.483	0.013520
pH of B-R solution (Q)	0.18846	1	0.18846	9.423	0.200487
(2) Modifier quantity (mg) (L)	6.22242	1	6.22242	311.121	0.036054
Modifier quantity (mg) (Q)	5.78937	1	5.78937	289.468	0.037375
(3) Scan rate (mV/s) (L)	1.27717	1	1.27717	63.858	0.079254
Scan rate (mV/s) (Q)	1.09350	1	1.09350	54.675	0.085577
1L by 2L	0.17761	1	0.17761	8.880	0.206114
1L by 3L	0.31681	1	0.31681	15.840	0.156711
2L by 3L	2.42881	1	2.42881	121.440	0.057612
Lack of Fit	1.47497	5	0.29499	14.750	0.195047
Pure Error	0.02000	1	0.02000		
Total SS	65.31178	15			

The observation of peaks at 2θ = 21.2° and 43.2° clearly indicate the presence of choline chloride agents on the surface of the GO sheets. However, no obvious diffraction peak of GO is observed. The possible mechanism is that the attached AuNPs prevent the restacking of these carbon sheets; therefore, the characteristic diffractions peaks of the layered structure disappear [49–52]. The results obtained by characterization techniques confirm that the AuNPs-ChCl-GO was successfully prepared.

3.2. Electrochemical behaviors of the prepared electrodes

The voltammetric measurements of CPE, GO/CPE, GO-ChCl/CPE, and AuNPs-ChCl-GO/CPE electrodes were performed towards the electrochemical sensing of MEL. The results in Fig. 6 demonstrate that optimum electrocatalytic efficiency is achieved by the AuNPs-ChCl-GO-based sensor. It is important to be noted that no measurable peak currents was observed without the presence of MEL in the studied potential range proving the performance of the sensor.

3.3. Evaluation of CCD model and interaction of input variables by RSM plots

In the optimization experiments, the 16 runs designed by CCD were carried out and the subsequent analysis by ANOVA predicted a second-order polynomial function as follows:

$$Y = 5.45524 - 3.50226X_1 - 0.33277X_1^2 + 1.22512X_2 + 1.42544X_2^2 - 0.71446X_3 + 0.53164X_3^2 - 0.29800X_1X_2 + 0.32805X_1X_3 + 1.11742X_2X_3$$

where, Y is the current (response), X_1 is the pH, X_2 is the modifier quantity and X_3 is the scan rate. The positive values indicate their positive effect on response and the magnitude of parameters effect can be evaluated.

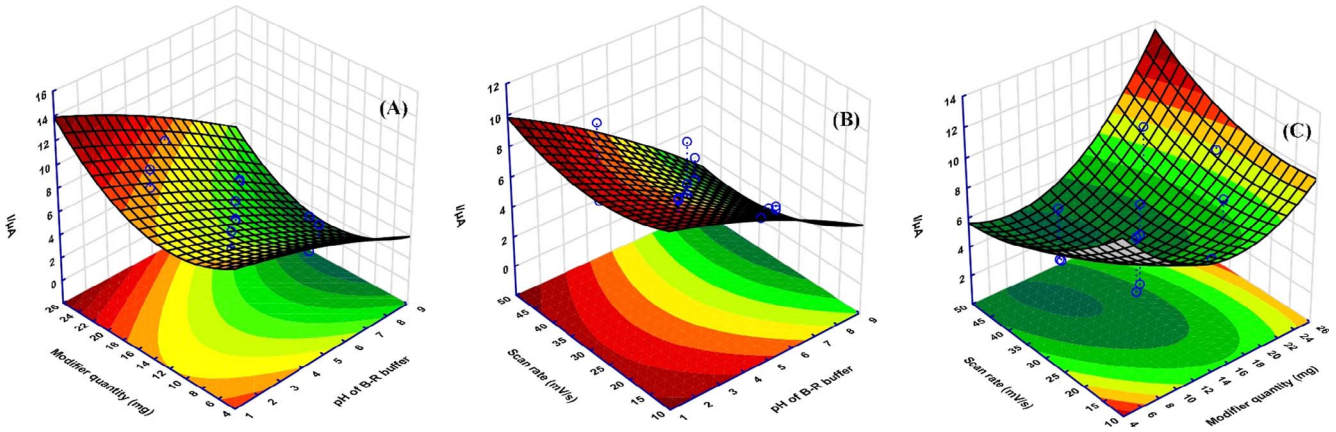

Fig. 8. Response surface plots of (A) pH versus modifier quantity (mg), (B) scan rate (mV/s) versus pH, and (C) scan rate (mV/s) versus modifier quantity for current response of biosensor.

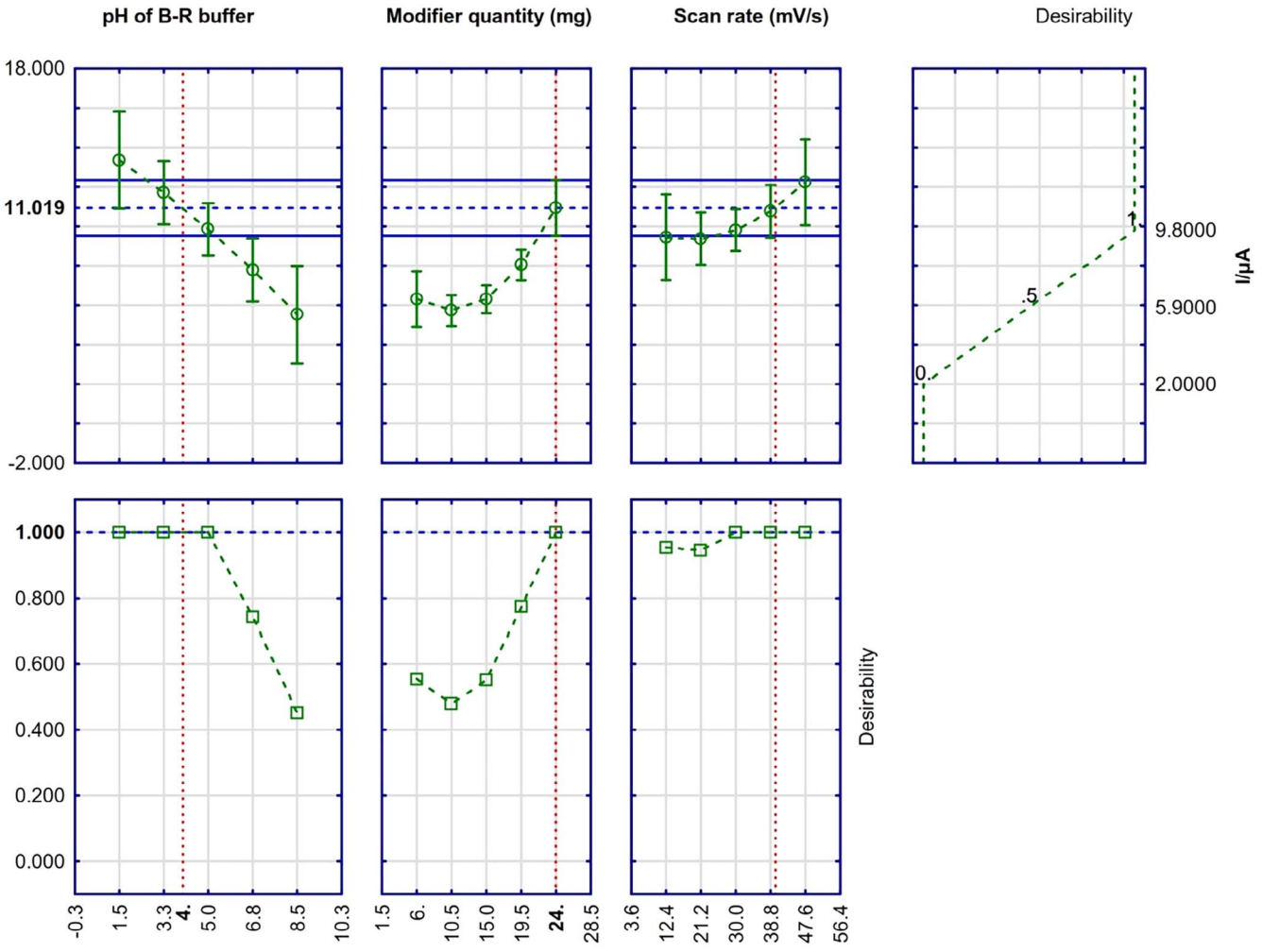

Fig. 9. Profiles for the observed, desirability function and predicated values for performance estimation of the AuNPs/ChCl/GO/CPE for MEL detection.

Fig. 7A illustrates a linear relationship between experimental data and fitted model, indicating normal distribution around the average response with minimum error. A predicted R^2-value of 97.50 is also achieved that is acceptable in comparison with the adjusted R^2-value of 94.00. The normal probability of residuals in Fig. 7B indicates that almost no serious deviation of the predicted data is seen in comparison with the experimental data after the analysis. Satisfactory normal distribution of the results confirm the suitability and applicability of the prediction.

Pareto chart was used to visualize the estimated effect of the variables. The chart in Fig. 7C shows the significant effects of X_1, X_2, X_2^2 on the peak current.

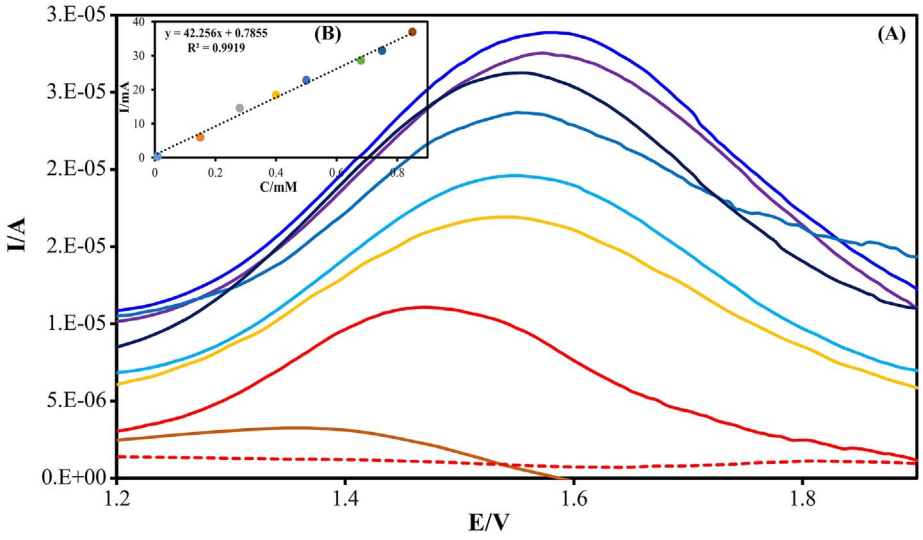

Fig. 10. (A) DPVs of MEL in the B–R buffer solution at pH = 4.0 containing different concentrations of MEL at a scan rate of 40 mV/s and (B) plot of the peak current as a function of MEL in the concentration range of 9.0×10^{-9} to 8.5×10^{-7} M.

Table 3
Quantitative results, precision and accuracy data for estimation of method validation.

DLR (μM)	LOQ (μM)	LOD (μM)	Repeatability Intra-day, RSD (n = 3) (0.01 μM)	Reproducibility Inter-day; RSD (n = 3) (0.01 μM)
0.009–0.85	1.008×10^{-9}	3.36×10^{-9}	2.05%	1.87%

As demonstrated in Table 2, all the observations is substantiated. The non-significant value of lack of fit represents validity of the quadratic model for explanation of the experimental data in present study. The interaction results obviously demonstrate higher efficacy of the linear terms of the pH and modifier quantity in comparison with the scan rate. Increasing modifier quantity to higher values has a positive effect on the response. In contrast, while the pH increases to higher values, negative response is obtained and no significant changes is seen at lower pH (Fig. 8). According to the desirability function in Fig. 9, the maximum response can be achieved using 24.0 mg modifiers at pH = 4.0 with a scan rate of 40 mV/s.

3.4. Analytical characterization and method validation

The solutions of AuNPs-ChCl-GO in the B-R buffer at pH = 4.0 containing various concentrations of MEL were used under optimized conditions to perform DPVs experiments. The variations of peak current versus MEL concentrations in Fig. 10 show a linear calibration curve with approximately two orders of magnitude in the concentration range of 9.0×10^{-9} to 8.5×10^{-7} M with the regression equation of I (μA) = 42.256 C(μM) + 0.7855 and R^2 = 0.9919. The limit of detection (LOD) and the limit of quantification (LOQ) were calculated according to signal to noise ratio (S/N) for three times and ten times, respectively, where, S is the standard deviation of the background. As can be seen in Table 3, LOD value is 1.008×10^{-9} M, while the LOQ value is 3.360×10^{-9} M. The results of intra-day and inter-day precisions are 2.05% and 1.87%, respectively. By storage of the electrode in the air for two weeks, no changes were seen in the peak current of the AuNPs-ChCl-GO electrode and it kept 90.0% of its initial response up to one month.

3.5. Application of the biosensor for real sample

To evaluate MEL concentration in the prepared human plasma sample, the AuNPs-ChCl-GO sensor was applied. The method of the plasma sample preparation was mentioned in Section 2.3.6. The standard addition calibration curve plotted for detection of MEL in real sample in Fig. 11 shows a straight line in the linear dynamic range with the regression equation of I (μA) = 98.26C + 9.57 and R^2 = 0.993. An average value of 0.508 μM was obtained for MEL in the plasma sample

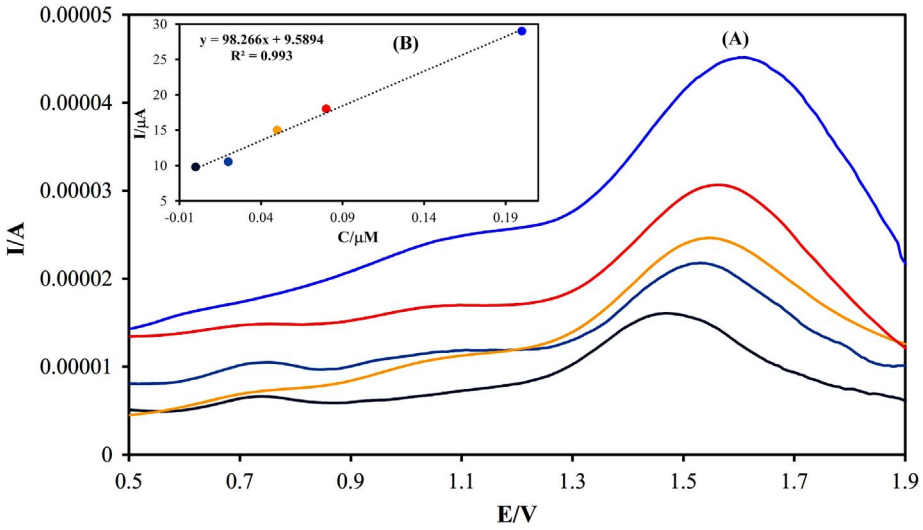

Fig. 11. (A) DPVs obtained by the AuNPs/ChCl/GO/CPE electrode as a function of standard MEL concentration added to the human plasma real samples in the range of 0.02–0.2 μM in the B-R buffer solution at pH = 4.0 and (B) standard-addition calibration plot from the data.

that is in good agreement with the spiked value. The results obtained in this study verify the efficacy of the proposed biosensor.

4. Conclusions

In this research study, a combination of AuNPs, choline chloride and grapheme oxide was produced, characterized by FTIR, TEM, FE-SEM, EDX, and XRD and then applied as novel bioelectrochemical sensor to investigate the electrochemical response towards MEL. CCD-RSM design used to improve MEL detection was successfully optimized the levels of parameters with a desirability function. According to the desirability function, the maximum response was achieved using 24.0 mg modifiers at pH = 4.0 with a scan rate of 40 mV/s. The linear relationship between experimental data and fitted model indicated normal distribution around the average response, confirming minimum error with acceptable R^2-value of 97.50 in comparison with the adjusted R^2-value of 94.00. The results showed that the storage of the electrode in the air for two weeks had no changes in the peak current of the AuNPs-ChCl-GO electrode and it kept 90.0% of its initial response up to one month. The application of the biosensor for real sample had an average value of 0.508 μM for MEL in the plasma sample that was in good agreement with the spiked value. The advantages including favorable low detection limit value, easy preparation and the long-time stability and reproducibility introduce the investigated biosensor as a very applicable and simple device for MEL detection in the presence of many interfering species in biological samples.

References

[1] Y. Yuan, X. Chen, D. Zhong, Determination of meloxicam in human plasma by liquid chromatography-tandem mass spectrometry following transdermal administration, J. chromatogr. B 852 (2007) 650–654.
[2] H.Y. Ji, H.W. Lee, Y.H. Kim, D.W. Jeong, H.S. Lee, Simultaneous determination of piroxicam, meloxicam and tenoxicam in human plasma by liquid chromatography with tandem mass spectrometry, J. chromatogr. B 826 (2005) 214–219.
[3] K.B. Liew, G.O. Loh, Y.T. Tan, K.K. Peh, Improved protein deproteinization method for the determination of meloxicam in human plasma and application in pharmacokinetic study, Biomed. Chromatogr. 28 (2014) 1782–1788.
[4] C.Y. Wang, Z.X. Wang, J. Guan, X.Y. Hu, Voltammetric determination of meloxicam in pharmaceutical formulation and human serum at glassy carbon electrode modified by cysteic acid formed by electrochemical oxidation of L-cysteine, Sensors 6 (2006) 1139–1152.
[5] S. Cox, J. Hayes, J. Yarbrough, T. Veiga-Parga, C. Greenacre, High-performance liquid chromatography determination of meloxicam and piroxicam with ultraviolet detection, Chromatogr. Res. Int. 2014 (2014) 1–7.
[6] E. Nemutlu, S. Kir, Validated determination of meloxicam in tablets by using UV spectrophotometry, Hacettepe Uni. J. Facul. Pharm. 24 (2004) 13–24.
[7] E. Nemutlu, S. Kir, Method development and validation for the analysis of meloxicam in tablets by CZE, J. Pharm. Biomed. Anal. 31 (2003) 393–400.
[8] S.E. Vignaduzzo, P.M. Castellano, T.S. Kaufman, Method development and validation for the simultaneous determination of meloxicam and pridinol mesylate using RP-HPLC and its application in drug formulations, J. Pharm. Biomed. Anal. 46 (2008) 219–225.
[9] S. Altinoz, E. Nemutlu, S. Kir, Polarographic behaviour of meloxicam and its determination in tablet preparations and spiked plasma, Farmaco 57 (2002) 463–468.
[10] G. Altiokka, Z. Atkosar, M. Tuncel, Pulse polarographic determination of meloxicam, Die Pharmazie 56 (2001) 184–185.
[11] L. Emara, M. Emam, N. Taha, H. Raslan, A. El-Ashmawy, A simple and sensitive HPLC/UV method for determination of meloxicam in human plasma for bioavailability and bioequivalence studies, J. Appl. Pharm. Sci. (2016) 012–019.
[12] L. Chen, H.T. Lian, X.Y. Sun, B. Liu, Sensitive detection of L-5-hydroxytryptophan based on molecularly imprinted polymers with graphene amplification, Anal. Biochem. 526 (2017) 58–65.
[13] C. Rajkumar, B. Thirumalraj, S.-M. Chen, S. Palanisamy, Novel electrochemical preparation of gold nanoparticles decorated on a reduced graphene oxide-fullerene composite for the highly sensitive electrochemical detection of nitrite, RSC Adv. 6 (2016) 68798–68805.
[14] Y. Yang, A.M. Asiri, Z. Tang, D. Du, Y. Lin, Graphene based materials for biomedical applications, Mater. Today 16 (2013) 365–373.
[15] D. Sharma, S. Kanchi, M.I. Sabela, K. Bisetty, Insight into the biosensing of graphene oxide: present and future prospects, Arab. J. Chem. 9 (2016) 238–261.
[16] J.I. Paredes, S. Villar-Rodil, A. Marti'nez-Alonso, J.M.D. Tasco'n, Graphene oxide dispersions in organic solvents, Langmuir 24 (2008) 10560–10564.
[17] M. Roosta, M. Ghaedi, A. Daneshfar, R. Sahraei, Ultrasound assisted microextraction-nano material solid phase dispersion for extraction and determination of thymol and carvacrol in pharmaceutical samples: experimental design methodology, J. Chromatogr. B 975 (2015) 34–39.
[18] C. Zhu, G. Yang, H. Li, D. Du, Y. Lin, Electrochemical sensors and biosensors based on nanomaterials and nanostructures, Anal. Chem. 87 (2015) 230–249.
[19] F. Chemat, H.J. You, K. Muthukumar, T. Murugesan, Effect of l-arginine on the physical properties of choline chloride and glycerol based deep eutectic solvents, J. Mol. Liq. 212 (2015) 605–611.
[20] G.-P. Jin, X.-Q. Lin, The electrochemical behavior and amperometric determination of tyrosine and tryptophan at a glassy carbon electrode modified with butyrylcholine, Electrochem. commun. 6 (2004) 454–460.
[21] P. Wang, Z. Mai, Z. Dai, Y. Li, X. Zou, Construction of Au nanoparticles on choline chloride modified glassy carbon electrode for sensitive detection of nitrite, Biosens. Bioelectron. 24 (2009) 3242–3247.
[22] L. Wang, E. Wang, Direct electron transfer between cytochrome c and a gold nanoparticles modified electrode, Electrochem. commun. 6 (2004) 49–54.
[23] J. Huang, Z. Xie, Z. Xie, S. Luo, L. Xie, L. Huang, Q. Fan, Y. Zhang, S. Wang, T. Zeng, Silver nanoparticles coated graphene electrochemical sensor for the ultrasensitive analysis of avian influenza virus H7, Anal. Chim. Acta 913 (2016) 121–127.
[24] W. He, Y. Liu, Z. Wan, C. Jia, Electrodeposition of V2O5 on TiO2 nanorod arrays and their electrochromic properties, RSC Adv. 6 (2016) 68997–69006.
[25] S.S. Miao, M.S. Wu, L.Y. Ma, X.J. He, H. Yang, Electrochemiluminescence biosensor for determination of organophosphorous pesticides based on bimetallic Pt-Au/multi-walled carbon nanotubes modified electrode, Talanta 158 (2016) 142–151.
[26] A. Suea-Ngam, P. Rattanarat, K. Wongravee, O. Chailapakul, M. Srisa-Art, Droplet-based glucosamine sensor using gold nanoparticles and polyaniline-modified electrode, Talanta 158 (2016) 134–141.
[27] A. Moghtada, R. Ashiri, Enhancing the formation of tetragonal phase in perovskite nanocrystals using an ultrasound assisted wet chemical method, Ultrason. Sonochem. 33 (2016) 141–149.
[28] K. Xu, Y. Wang, X. Ding, Y. Huang, N. Li, Q. Wen, Magnetic solid-phase extraction of protein with deep eutectic solvent immobilized magnetic graphene oxide nanoparticles, Talanta 148 (2016) 153–162.
[29] D.R. Dreyer, S. Park, C.W. Bielawski, R.S. Ruoff, The chemistry of graphene oxide, Chem. Soc. Rev. 39 (2010) 228–240.
[30] M.A. Mohamed, A.M. Yehia, C.E. Banks, N.K. Allam, Novel MWCNTs/graphene oxide/pyrogallol composite with enhanced sensitivity for biosensing applications, Biosens. Bioelectron. 89 (2017) 1034–1041.
[31] S. Bahrani, M. Ghaedi, M.J. Khoshnood Mansoorkhani, A. Ostovan, A highly selective nanocomposite based on MIP for curcumin trace levels quantification in food samples and human plasma following optimization by central composite design, J. Chromatogr. B 1040 (2017) 129–135.
[32] A. Asfaram, M. Ghaedi, M.K. Purkait, Novel synthesis of nanocomposite for the extraction of Sildenafil Citrate (Viagra) from water and urine samples: process screening and optimization, Ultrason. Sonochem. 38 (2017) 463–472.
[33] A. Ostovan, M. Ghaedi, M. Arabi, A. Asfaram, Hollow porous molecularly imprinted polymer for highly selective clean-up followed by influential preconcentration of ultra-trace glibenclamide from bio-fluid, J. Chromatogr. A 1520 (2017) 65–74.
[34] G.B.B. Varadwaj, O.A. Oyetade, S. Rana, B.S. Martincigh, S.B. Jonnalagadda, V.O. Nyamori, Facile synthesis of three-dimensional Mg-Al layered double hydroxide/partially reduced graphene oxide nanocomposites for the effective removal of Pb2+ from aqueous solution, ACS Appl. Mater. Interfaces 9 (2017) 17290–17305.
[35] E. Kazemi, S. Dadfarnia, A.M. Haji Shabani, A. Abbasi, M.R. Rashidian Vaziri, A. Behjat, Iron oxide functionalized graphene oxide as an efficient sorbent for dispersive micro-solid phase extraction of sulfadiazine followed by spectrophotometric and mode-mismatched thermal lens spectrometric determination, Talanta 147 (2016) 561–568.
[36] Z. Li, F. Chen, L. Yuan, Y. Liu, Y. Zhao, Z. Chai, W. Shi, Uranium(VI) adsorption on graphene oxide nanosheets from aqueous solutions, Chem. Eng. J. 210 (2012) 539–546.
[37] W.H. Kong, D.K. Sung, K.S. Kim, H.S. Jung, E.J. Gho, S.H. Yun, S.K. Hahn, Self-assembled complex of probe peptide–E–Coli RNA I conjugate and nano graphene oxide for apoptosis diagnosis, Biomaterials 33 (2012) 7556–7564.
[38] E. Roy, S. Patra, D. Kumar, R. Madhuri, P.K. Sharma, Multifunctional magnetic reduced graphene oxide dendrites: synthesis, characterization and their applications, Biosens. Bioelectron. 68 (2015) 726–735.
[39] X. Mei, J. Ouyang, Ultrasonication-assisted ultrafast reduction of graphene oxide by zinc powder at room temperature, Carbon 49 (2011) 5389–5397.
[40] M. Arabi, M. Ghaedi, A. Ostovan, S. Wang, Synthesis of lab-in-a-pipette-tip extraction using hydrophilic nano-sized dummy molecularly imprinted polymer for purification and analysis of prednisolone, J. Colloid Interface Sci. 480 (2016) 232–239.
[41] S. Bahrani, M. Ghaedi, M.J. Mansoorkhani, A. Asfaram, A.A. Bazrafshan, M.K. Purkait, Ultrasonic assisted dispersive solid-phase microextraction of Eriochrome Cyanine R from water sample on ultrasonically synthesized lead (II) dioxide nanoparticles loaded on activated carbon: experimental design methodology, Ultrason. Sonochem. 34 (2017) 317–324.
[42] A. Asfaram, M. Ghaedi, Simultaneous determination of cationic dyes in water samples with dispersive liquid–liquid microextraction followed by spectrophotometry: experimental design methodology, New J. Chem. 40 (2016) 4793–4802.
[43] M.H. Omidi, F.N. Azad, M. Ghaedi, A. Asfaram, M.H.A. Azqhandi, L. Tayebi, Synthesis and characterization of Au-NPs supported on carbon nanotubes: application for the ultrasound assisted removal of radioactive UO22+ ions following complexation with Arsenazo III: spectrophotometric detection, optimization, isotherm and kinetic study, J. Colloid Interface Sci. 504 (2017) 68–77.
[44] J. Bhatt, D. Mondal, K. Prasad, Experimental evidence for the participation of deep eutectic solvents in silver chloride crystal formation at low temperature, J. Cryst. Growth 442 (2016) 95–97.

[45] L. Vieira, R. Schennach, B. Gollas, In situ PM-IRRAS of a glassy carbon electrode/deep eutectic solvent interface, Phys. Chem. Chem. Phys. 17 (2015) 12870–12880.
[46] L. Alidokht, S. Oustan, A. Khataee, M.R. Neyshabouri, A. Reyhanitabar, Enhanced removal of chromate by graphene-based sulfate and chloride green rust nanocomposites, J. Taiwan Inst. Chem. Eng. 68 (2016) 266–274.
[47] M. Hayyan, A. Abo-Hamad, M.A. AlSaadi, M.A. Hashim, Functionalization of graphene using deep eutectic solvents, Nanoscale Res. Lett. 10 (2015) 1004.
[48] A. Kaveh, A. ArefAzar, Surface modification of graphene oxide and investigation of its effects on surface properties of aramid membranes, Polym. Plast. Technol. Eng. 54 (2015) 1606–1614.
[49] P. Kar, S. Sardar, B. Liu, M. Sreemany, P. Lemmens, S. Ghosh, S.K. Pal, Facile synthesis of reduced graphene oxide-gold nanohybrid for potential use in industrial waste-water treatment, Sci. Technol. Adv. Mater. 17 (2016) 375–386.
[50] J. Wang, P. Yang, M. Cao, N. Kong, W. Yang, S. Sun, Y. Meng, J. Liu, A novel graphene nanodots inlaid porous gold electrode for electrochemically controlled drug release, Talanta 147 (2016) 184–192.
[51] X. Du, Z. Zhang, Z. Miao, M. Ma, Y. Zhang, C. Zhang, W. Wang, B. Han, Q. Chen, One step electrodeposition of dendritic gold nanostructures on beta-lactoglobulin-functionalized reduced graphene oxide for glucose sensing, Talanta 144 (2015) 823–829.
[52] G. Jalani, M. Cerruti, Nano graphene oxide-wrapped gold nanostars as ultrasensitive and stable SERS nanoprobes, Nanoscale 7 (2015) 9990–9997.